Journal of Food Process Engineering

WILEY

Journal of Food Process Engineering

ORIGINAL ARTICLE OPEN ACCESS

Influence of Pressure Holding Time on Ovalbumin Solution Behavior via Small-Angle Neutron Scattering and Diffusing Wave Spectroscopy

Brian Paul[1,2] | Eric M. Furst[1] | Abraham M. Lenhoff[1] | Elliot P. Gilbert[3] | Norman J. Wagner[1] | Susana C. M. Teixeira[1,2]

[1]Center for Neutron Science, Department of Chemical and Biomolecular Engineering, University of Delaware, Delaware, USA | [2]NIST Center for Neutron Research, National Institute of Standards and Technology, Gaithersburg, Maryland, USA | [3]Australian Centre for Neutron Scattering, Australian Nuclear Science and Technology Organization, Kirrawee DC, New South Wales, Australia

Correspondence: Susana C. M. Teixeira (susanat@udel.edu)

Received: 15 November 2024 | **Revised:** 13 January 2025 | **Accepted:** 17 March 2025

Funding: This work was supported by NIST Center for Neutron Research; Australian Nuclear Science and Technology Organisation.

Keywords: diffusing-wave spectroscopy | high pressure | salt additives | small-angle neutron scattering | viscosity

ABSTRACT

Protein–protein interactions (PPIs) were characterized as a function of salt concentration and applied hydrostatic pressure for hen egg ovalbumin solutions. In situ data were collected using small-angle neutron scattering (SANS) at various concentrations of ammonium sulfate. The nondestructive nature of SANS allows for extended pressure holding times and the investigation of the reversibility of effects on PPIs. An empirical scaling developed previously is shown to capture the dependence of the reduced osmotic second virial coefficient on an effective pressure, combining osmotic and hydrostatic contributions. A comparison to small-angle X-ray scattering data for ovalbumin indicates enhanced net attraction at all conditions investigated with longer pressure holding times. Pressure effects on PPIs measured by SANS are shown not to be fully reversible in the presence of salt. Pressure-triggered aggregation was detected in the hours after depressurization at moderate salt concentrations, with slow recovery of pressure-induced attraction at high salt concentrations. Consistency is demonstrated between predicted solution viscosities and experimental observations from viscometry and in situ high-pressure diffusing wave spectroscopy. Furthermore, both the strength of ovalbumin PPIs and the relative solution viscosity display Barus-like scaling with effective pressure, exhibiting distinct pressure-viscosity coefficients from those of water.

1 | Introduction

Food processing relies on the careful control of composition, morphology, and product stability (Allai et al. 2023). Successful manipulation of food properties requires tuning multiple intrinsic and extrinsic parameters, including target pressure, temperature, pH, and salt addition. High-pressure (HP) processing is a noninvasive treatment that provides an alternative to traditional thermal or additive-based steps (Rastogi 2013; Wimalaratne and Farid 2008). Although hydrostatic pressure is instantly felt across the entire product volume, the direct or indirect effects of pressure, such as partial protein unfolding or the dissociation of protein oligomers, can trigger relatively slow irreversible processes (Charlier et al. 2018; Moron et al. 2022). Furthermore, protein behavior has a known dependence on pressure holding time (Xu et al. 2021), with reported time scales for HP processing of a few seconds to 30 min or more (Amsasekar et al. 2022; Ngamlerst et al. 2022).

A prior investigation of protein–protein interactions (PPIs) revealed an empirical master scaling curve between pressure and salt effects on the reduced second virial coefficient of hen egg protein ovalbumin solutions (Paul et al. 2023), and successfully applied to data available in the literature for other proteins and salts. The study was based on high-pressure small-angle X-ray scattering (HP-SAXS) data collected on samples incubated at a series of steps at increasing pressure, for no more than 5 min/step to mitigate the accumulation of radiation damage effects (Hopkins and Thorne 2016). The work described here uses high-pressure small-angle neutron scattering (HP-SANS) to access longer pressure incubation time and to investigate the reversibility of pressure effects, while ensuring consistency between measurements taken on the same sample (Teixeira 2019). Ovalbumin is a well-characterized food protein used in numerous products for its emulsifying, gelling, and stabilizing properties (Chen et al. 2024; Rostamabadi et al. 2023). Despite its allergenicity, the nutritional and functional uniqueness of ovalbumin granted research towards its animal-free production as a more sustainable protein-sourcing alternative (Diwan et al. 2021). Of note, several nonthermal treatments have been shown to mask or destroy allergenic protein epitopes, including high pressure (Dong et al. 2024).

Ovalbumin has an isoelectric point of 4.5 (Abeyrathne et al. 2013). At neutral pH, a net charge of −11 e has been reported (Ianeselli et al. 2010). In the absence of salt, PPIs in the dilute or semi-dilute regimes are dominated by electrostatic repulsion because of the long-range nature of the interactions, a major contributor to solution viscosity. Controlling the viscosity of protein solutions is a present-day technological challenge, often addressed by modulating the difference between pH and protein pI, as well as by using small-solute additives such as salts. The use of pressure is of interest in this context (Abbas et al. 2010), as well as at a more fundamental level, to understand the molecular-basis for PPIs and develop predictive tools at various concentration regimes. Previous studies reported temperature effects on the zero-shear viscosity of albumins in water (Monkos 2000) and in salt-containing solutions (Heinen et al. 2012) but high-pressure viscosity has been minimally explored. In-situ data for β-lactoglobulin (Marjanović et al. 2011), measured using a rolling ball viscometer, indicated a non-linear increase in viscosity with applied pressure up to 600 MPa. A different, minimally invasive, option for accessing rheological behavior is passive microrheology, which does not require external forces acting on the sample of interest (Josephson et al. 2016; McGlynn et al. 2020). Diffusing wave spectroscopy (DWS) is a light-scattering based passive microrheology technique that is sensitive to weak responses compared with bulk rheology. To our knowledge, however, there have been no reported applications of HP-DWS to protein solutions. Pressure effects on viscosity are well known, especially in the lubrication field, where viscosity behavior has often been modeled using the empirical Barus equation (Barus 1893) for pressures below 1 GPa. Pressure-viscosity coefficients α are on the order of $10^{-2}\,MPa^{-1}$ for lubricants (Hayashi et al. 2008), $10^{-3}\,MPa^{-1}$ for polymer melts (Couch and Binding 2000) and $10^{-4}\,MPa^{-1}$ for water. Foods with high water content or dilute solutions are expected to follow similar pressure-viscosity scaling to that of water (Först et al. 2002).

The work described here uses HP-SANS to map ovalbumin PPIs in the presence of ammonium sulfate, a salt commonly used in foods. The interactions are quantified by the reduced osmotic second virial coefficient b_2^* under pressure incubation times relevant to pressure processing (Knorr 2002). b_2^* is related to the interaction free energy averaged over all orientations and separations between a pair of proteins, normalized by an excluded volume contribution. The reversibility of pressure effects was investigated up to 24 h after depressurization. 20 min pressure holding effects were used within the framework of colloidal rheology to predict solution viscosity across the range of pressures and salt concentrations investigated. These were directly compared to experimental observations from viscometry and in situ high-pressure DWS (HP-DWS). Building on our prior work, we identify a Barus-like scaling for protein solution relative viscosity and effective pressure. The relative viscosity of proteins in dilute solutions is defined as solution viscosity normalized by the buffer viscosity. It is an indirect measure of PPIs and can be used to fine-tune colloidal stability (Boonyaratanakornkit et al. 2002; Winter 2015).

2 | Materials and Methods

2.1 | Sample Preparation

Ammonium sulfate (AS), sodium phosphate monobasic anhydrous, and lyophilized ovalbumin with purity ≥98% (agarose gel electrophoresis; A5503) were purchased from Sigma-Aldrich (Merck, Melbourne, VIC, Australia; and Millipore-Sigma, St. Louis, MO). Ovalbumin was used without further purification. Sodium deuteroxide from Cambridge Isotope Laboratories (Andover, MA) was used to adjust the pH to 7 in D_2O-based buffers. The measured pH was taken as directly equivalent to pD. Polystyrene (PS) microspheres were purchased with a diameter of 0.29 µm and a mass to volume fraction of 5% PS (Spherotech, Lake Forest, IL). Pluronic F-127 (mass fraction of 1% in water) and toluene were purchased from Fisher Scientific (Pittsburg, PA).

Ovalbumin samples were prepared as described previously (Paul et al. 2023). Briefly, stock solutions of 2.4 M AS were prepared by dissolving the salt in 5 mM phosphate buffer at pD 7. Lower AS concentration solutions were prepared by dilution of the stock with phosphate buffer. Ovalbumin powder was directly solubilized in each buffer solution to produce a nominal concentration of 10 mg/mL, confirmed via absorbance at 280 nm ($E_{1cm}^{\%} = 7.35\,g\,cm^{-1}\,/\,100\,mL$) (Lundblad and Macdonald 2018). Samples were prepared no more than 24 h prior to HP-SANS data collection.

Prior to dispersing into the DWS samples, the PS tracer particles were sterically stabilized for use at high salt concentrations, through a previously reported swelling procedure (Kim et al. 2005). Briefly, a slight excess volume of Pluronic F-127 (129 mL) was mixed with 8.4 mL of PS stock solution via gentle stirring for 12 h. The suspension was mixed with a volume of toluene equal to the total polystyrene volume in the suspension (0.4 mL) and stirred for an additional 12 h. It should be noted that the chosen ratio of toluene to PS volumes prevents water-toluene emulsification during the procedure. Toluene is a good solvent for polystyrene, allowing F-127 brushes to penetrate the tracer interface, preventing the swollen PS particles from coalescing. To strip the solvent and de-swell the particles, the suspension was then heated at 95°C for 30 min in an open container using a water bath. It was then cooled to room temperature and concentrated via centrifugation (4300 rpm for 30 min). Excess F-127 was removed with the supernatant and the PS tracers were re-dispersed in ultrapure water (18.2 MΩ cm, Milli-Q) to produce a concentrated stock solution. Prior to each microrheology experiment, three 1.4 mL aliquots of concentrated tracer PS stock were additionally washed five times via centrifugation to remove trace F-127 (2350 rpm for 30 min). After each wash, 1.3 mL of supernatant were discarded, and particles were resuspended in 1.2 mL of ultrapure water. After the final wash, PS tracers were resuspended in phosphate buffer. The nominal particle size before and after grafting was confirmed using dynamic light scattering (DLS; Zetasizer Nano, Malvern Panalytical), with a final grafted particle diameter of ~310 nm, which did not change after each washing step. Grafting was additionally confirmed by observing a 90% reduction in the tracer ζ-potential after the swelling procedure. The decreased ζ-potential after grafting is indicative of good surface coverage of polymer brushes on the tracer particles (Garting and Stradner 2018). The tracer aliquots were then combined with the appropriate volumes of ovalbumin AS solution to produce 40 mL solution containing 10 mg/mL ovalbumin at the desired salt concentration and a volume fraction of 0.5% PS tracer particles. Tracer suspensions in a 4:1 mixture by volume of 2-propanol:water were prepared similarly, as control samples (Figure S8).

2.2 | In Situ Ambient- and High-Pressure Small-Angle Neutron Scattering

SANS measurements on 5 mg/mL ovalbumin solution (0 M AS) were collected at ambient pressure using the NG7 30 m instrument (Glinka et al. 1998) of the NIST Center for Neutron Research (NCNR; Maryland, USA). Three instrument configurations with a neutron wavelength of $\lambda = 6$ Å, and one configuration at $\lambda = = 8.1$ Å using neutron focusing lenses, provided a total accessible momentum transfer Q-range of 0.001 Å^{-1}—0.7 Å^{-1}. Q is defined as:

$$Q = \frac{4\pi}{\lambda} \sin\theta \tag{1}$$

and the scattering angle is 2θ. A 640 mm × 640 mm 2D position-sensitive detector with 128 pixels × 128 pixels (5.08 × 5.08 mm^2 per pixel). Data reduction was carried out using Igor Pro (Wavemetrics, Lake Oswego, OR) and the NCNR SANS reduction package (Kline 2006). Raw counts were corrected for empty cell, ambient background, and non-uniform detector sensitivity contributions. Data were placed on an absolute scale by normalizing the scattering intensity to the incident beam flux. Buffer scattering was measured for salt-free solution and subtracted from the corresponding ovalbumin solution scattering data. Data were fitted using SasView (Doucet et al. 2022) using a triaxial ellipsoid form factor averaged over all orientations (Finnigan and Jacobs 1971)—see also Supporting Information: Section 1. Guinier analyses—see also Figure S1 and Tables S1 and S2—reveal a radius of gyration of $R_g = 22.1$ Å ± 0.2 Å for 5 mg/mL ovalbumin solutions in the absence of AS, in good agreement with ambient pressure data collected on the 40 m QUOKKA beamline (21.2 Å ± 0.2 Å) at the Australian Center for Neutron Scattering (Wood et al. 2018).

SANS measurements on 10 mg/mL protein solutions of varying AS concentration were also performed on the QUOKKA instrument (see Figure 1). In situ HP-SANS data were collected using a McHugh-type high-pressure cell, based on the design of the pressure system available at the NCNR (Teixeira et al. 2018). Data were collected at $\lambda = 5$ Å with a 10% wavelength spread. Two instrument configurations were used to access a Q-range of 0.006 Å^{-1}–0.22 Å^{-1}. The data were recorded on a 960 mm × 960 mm multi-wire ^{3}He proportional detector with 5 × 5 mm^2 resolution per pixel, collected sequentially across a series of pressure conditions. Specifically, steps of P (MPa): 0.1, 100, 200, 250, 300, 0.1, where 0.1 MPa is the nominal ambient pressure at the beginning and end of the series. A 20 min incubation period was used before scattering data were recorded at each pressure step. The high-Q limit was restricted by the geometry of the pressure cell, but ambient pressure data were additionally collected in quartz banjo cells, to provide a reference for ambient pressure data over an extended Q range of 0.006 Å^{-1}–0.72 Å^{-1}. Data reduction was carried out using an adaptation of the Igor Pro NCNR macros for QUOKKA-specific parameters. Buffer scattering was approximated as a flat background contribution and subtracted from the corresponding ovalbumin solution data. Data were fitted as described previously (Paul et al. 2023). Briefly, the structure factor for the AS-free solutions was determined directly from the experimental data, by normalizing the 10 mg/mL ovalbumin SANS data with the 5 mg/mL solution data, based on the assumption that the form factor $P(Q)$ is the same at both concentrations. It was also assumed that the lowest concentration data has negligible structure factor contributions (see also Figure S2). The neutron-scattered intensities are described by:

$$I(Q) = V_f (\Delta\rho)^2 \, V \, P(Q) \, S_{eff}(Q) \tag{2}$$

where V_f is the volume fraction of ovalbumin in solution and $\Delta\rho$ is the difference between the neutron scattering length densities (SLDs) of the protein and the buffer. V is the specific volume of the protein, $P(Q)$ is the single-particle form factor and $S_{eff}(Q)$ is an effective structure factor that accounts for polydispersity and anisotropy of the ovalbumin solution structure, (Kotlarchyk and Chen 1983). The experimentally-determined structure factor was then used to determine b_2^*, estimated from the zero-angle structure factor $S(0)$ using (Goldenberg and Argyle 2014):

$$b_2^* = \left[\frac{1}{S(0)} - 1\right] \cdot \frac{3}{4} \, \frac{M_W}{\sigma^3 \pi C_p N_A} \tag{3}$$

where C_p is the protein concentration, N_A is Avogadro's number and M_W is the protein molar mass. The hard-sphere diameter σ can be approximated as twice the hydrodynamic radius, which was determined via DLS. $S(0)$ was determined for each AS-free solution scattering data set by averaging the value of the structure factor for $Q < 0.025$ Å^{-1}.

Version of Record at: https://doi.org/10.1111/jfpe.70088

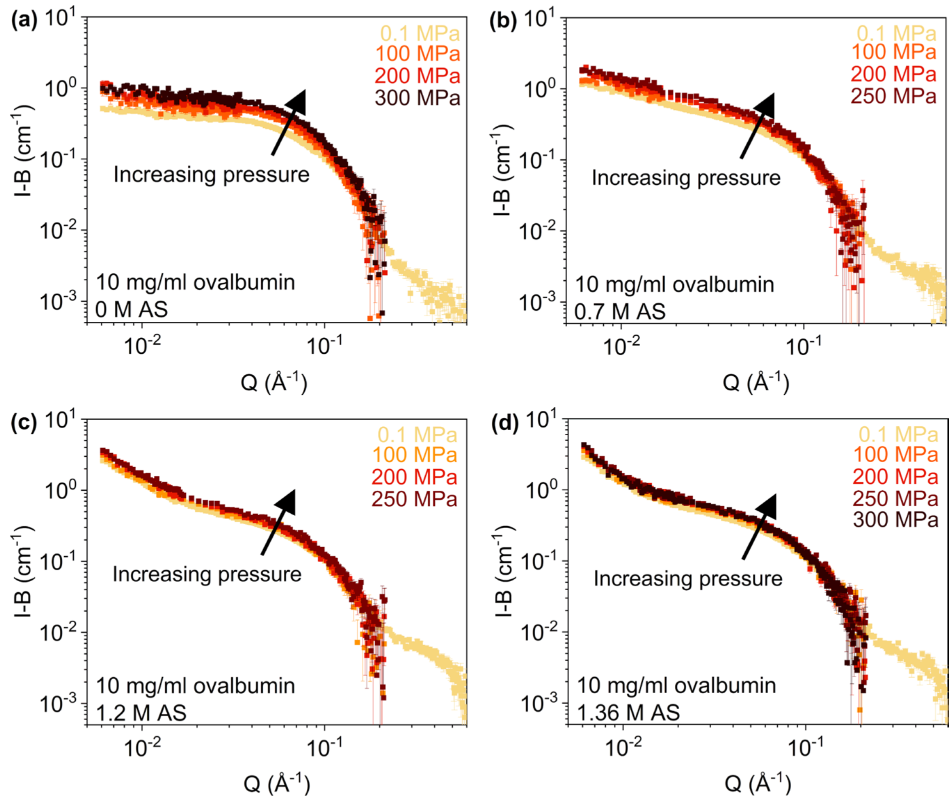

FIGURE 1 | HP-SANS intensity profiles (background-subtracted) of 10 mg/mL ovalbumin solutions containing (a) 0 M AS, (b) 0.7 M AS, (c) 1.2 M AS, and (d) 1.36 M AS. The applied pressure steps are shown, with darker shades indicating higher applied pressure. For 0.7 M and 1.2 M AS solutions, a leak in the pressure cell and beamtime limitations prevented data collection at 300 MPa. SANS data measured in banjo cells at ambient pressure (0.1 MPa) extend to higher Q than the pressure cell data. Error bars are standard errors from counting statistics and where not apparent are smaller than the symbol size.

For AS-containing solutions, the form factor was fitted with a triaxial ellipsoid. The structure factor was fitted with sticky hard spheres, a model that assumes attractive PPIs and would therefore not be applicable to the AS-free solutions (see also Figure S3). b_2^* for AS-containing solutions can be described at each applied pressure as a function of the Baxter stickiness parameter, τ_B (Wagner and Mewis 2012):

$$b_2^* = 1 - \frac{1}{4\tau_B} \tag{4}$$

using a "sticky" hard-sphere model based on the assumption that repulsive interactions are screened by salt counterions. b_2^* data were scaled as a function of a total effective pressure P_{eff} and directly compared with short-time behavior measured via HP-SAXS (Paul et al. 2023). Briefly, the osmotic coefficient ϕ was used to account for non-idealities in concentrated electrolyte solutions, so that the osmotic pressure can be defined as (Ullner et al. 2018):

$$\Pi = \frac{iC_sRT}{\phi} \tag{5}$$

where C_s is the salt concentration, T is the solution temperature, R is the gas constant and i is the number of moles of counterion per mole of salt. To combine the effects of salt and applied hydrostatic pressure, the total effective pressure on the protein in solution was defined as:

$$P_{eff} = P_{\text{applied}} + G\Pi \tag{6}$$

where P_{applied} is the applied hydrostatic pressure for the in situ HP-SANS measurements, and G is an empirical weighting parameter on the osmotic pressure contributions. G was determined by fitting b_2^* as a function of P_{applied} and Π using a numerical approach to parametrize the data, as previously reported (Paul et al. 2023) and further detailed in Supporting Information: Section 4. The master curve fit parameters were estimated using the MATLAB Curve Fitter (MathWorks, 2023). The goodness of fit was determined as $R^2 = 1$—RSS, where RSS is the sum of the squares due to error between experimental and fitted values, using a linear regression analysis normalized by the total sum of squares. $R^2 > 0.7$ was taken as an acceptable fit and $R^2 > 0.9$ as a good fit.

2.3 | High-Pressure Diffusing Wave Spectroscopy (HP-DWS)

Passive microrheology techniques use the Brownian motion of tracer particles dispersed in a sample fluid to determine rheological sample properties (Furst and Squires 2017). HP-DWS data were collected in transmission mode using a high-pressure microrheology instrument to measure viscoelastic behavior up to 207 MPa (Dennis et al. 2020). An argon ion laser (Innova 90C-5) point source was operated in single-frequency mode with a vacuum wavelength of $\lambda = 514.5\,\text{nm}$. The mean squared displacement (MSD) of the tracer particles can be directly calculated from the scattered intensity autocorrelation function (see Supporting Information: Section 8). Once the MSD is known, the zero-shear viscosity can be determined from the Stokes–Einstein–Sutherland equation:

$$D_0 = \frac{k_B T}{6\pi\, a\, \eta_0} \tag{7}$$

where, in three-dimensional space, $MSD = 6 D_0 \tau$. D_0 is the particle diffusivity, T is temperature, τ is the lag time characterizing the time-scale of particle motion, k_B is Boltzmann's constant, a is the tracer particle hydrodynamic radius, and η_0 is the zero-shear viscosity. Substituting and solving for η_0 yields:

$$\eta_0 = \frac{k_B\, T\, \tau}{\pi\, a\, MSD} \tag{8}$$

Finally, the pressure dependence of the viscosity can be described by the Barus equation (Barus 1893):

$$\eta(P) = \eta_0 e^{\alpha P} \tag{9}$$

where P is the applied pressure and α is the pressure-viscosity coefficient, with larger coefficients denoting a stronger pressure dependence of viscosity. The volume fraction of 0.5% tracer particles yields a scattering mean free path of multiple scattering of $l^* \approx 0.550\,\text{mm}$. The ratio of sample path length to scattering mean free path is $11.8 / l^* \approx 21$. A range of $4.5 < L / l^* < 50$ is desired to satisfy the diffusion approximation, that is, isotropic multiple scattering of photons through the sample (Weitz and Pine 1993). Pressure was applied at ambient temperature, from atmospheric pressure up to 200 MPa in increments of 50 MPa, with a final measurement after returning to ambient pressure (denoted as R0.1 MPa). Samples were incubated at each target pressure step for 20 min prior to HP-DWS data collection. The sample refractive indices (see also Figure S7) were measured in the absence of tracers (Abbemat 300 digital refractometer; Anton Paar, Graz, Austria). Tracers modified as described in 2.1 are colloidally stable in solutions up to 0.7 M AS but aggregate in the presence of higher AS concentrations within 1 h and microrheology was not measured for these solutions. Tracer colloidal stability up to 0.7 M AS buffer was confirmed, by measuring particle size over time via DLS using a 3D spectrometer (LS Instruments, Fribourg, Switzerland). The corresponding hydrodynamic radius as a function of time was then calculated by solving Equation (7).

2.4 | Capillary Viscometry

Data were collected on a Ubbelohde-type capillary viscometer at ambient temperature (24°C) for ovalbumin solutions and the corresponding protein-free buffers, at various AS concentration. The efflux time t_{efflux} between two markings on the capillary was measured—see also Table S6—to determine the solution kinematic viscosity:

$$\nu = C_K\, t_{efflux} \tag{10}$$

where $C_K = 0.003620$ is the viscometer constant for the capillary used (50-B507). The solution density ρ was determined using a DDM 2911 Plus Automatic Density Meter (Rudolph Research Analytical, Hackettstown, USA). The dynamic viscosity μ was then determined as:

$$\mu = \nu\, \rho \tag{11}$$

where μ was taken as equivalent to the zero-shear viscosity, η_0.

2.5 | Predicting Solution Viscosity From Protein Interactions

Macroscopic rheological solution behavior can be predicted for the ovalbumin solutions as (Wagner and Mewis 2012):

$$\eta_r = 1 + 2.5 V_f + \left(5.9 + \frac{1.9}{\tau_B}\right) V_f^2 \tag{12}$$

where $\eta_r = \eta_0 / \eta_s$ is the relative viscosity of the protein solution with respect to the buffer solution and V_f is the protein volume fraction. The predicted viscosity values for the 10 mg/mL ovalbumin solutions in various AS concentrations were directly compared to experimental observations from capillary viscometry (0.1 MPa, 0 M—1.36 M AS solutions) and from HP-DWS (0.1 MPa–200 MPa pressures, 0 M–0.7 M AS solutions).

3 | Results and Discussion

3.1 | Pressure Dependence of Protein Interactions From Small-Angle Neutron Scattering

HP-SANS data for 10 mg/ml ovalbumin solutions are shown in Figure 1. SANS intensity profiles scale with applied pressure due to differences between protein and water compressibility, as well as slight variations of the sample path length under pressure (Teixeira et al. 2018). Ambient pressure measurements in quartz banjo cells agree well with data collected at 0.1 MPa prior to pressurization (Table S2). The slope of the Q-dependence of the scattering intensities at low Q increases with applied pressure or AS concentration, particularly for $Q < 0.05\,\text{Å}^{-1}$. In the absence of AS, the scattering profile at ambient pressure reflects a small contribution of the structure factor centered at $Q \approx 0.02\,\text{Å}^{-1}$ (see also Figure S3), consistent with repulsive interactions. In the presence of AS, 10 mg/mL ovalbumin solutions in D_2O have a known ambient pressure aggregation boundary at ≈2 M AS (Dumetz et al. 2008; Greene et al. 2015) and a contribution to scattering from aggregates or oligomers is expected at lower AS concentrations as well. This is in agreement with prior HP-SAXS results (Paul et al. 2023). It should be noted that there is an additional contribution to the scattering data from an instrumental artifact to the lower Q intensities (measurable also in the empty beam scattering data, collected without sample or pressure cell present). For this reason, scattering intensities for $Q < 0.015\,\text{Å}^{-1}$ were not used in fitting any of the HP-SANS curves.

Figure 2a shows the effect of applied hydrostatic pressure on b_2^* for each AS concentration. As previously observed via

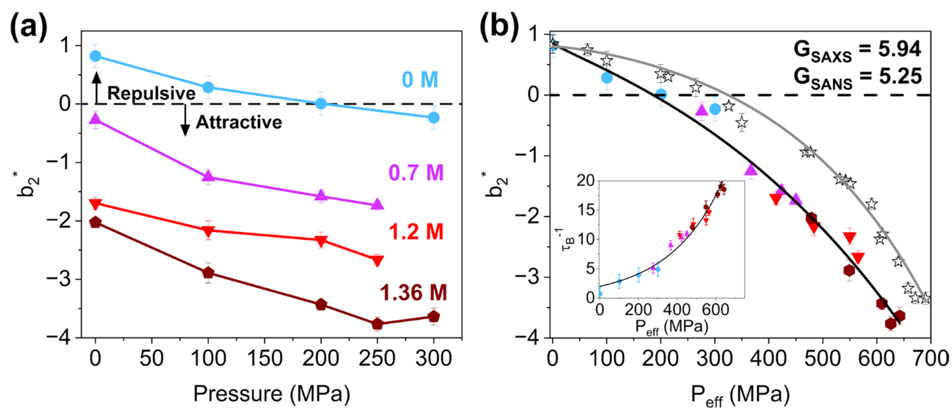

FIGURE 2 | (a) Reduced second virial coefficients b_2^* as a function of applied pressure, measured by HP-SANS for 10 mg/mL ovalbumin solutions at various AS-concentrations. The lines are guides for the eye. Error bars are estimated from the uncertainty in the hydrodynamic diameter (AS-free solutions) (Goldenberg and Argyle 2014) or are estimated from the fitting error in the Baxter stickiness parameter, τ_B. (b) Master curves of ovalbumin b_2^* as a function of effective pressure, following the same color scheme. HP-SANS data collected after 20 min of pressure incubations are shown by filled symbols, while HP-SAXS data collected after 5 min of pressure incubations (Paul et al. 2023) are shown as open black stars. Inset: Inverse of the Baxter stickiness parameter as a function of effective pressure. The fit line is to the Barus equation as shown. See also Tables S3 and S4.

HP-SAXS (Paul et al. 2023), b_2^* decreases with increasing AS concentration or applied pressure. Notably, in the absence of salt, the HP-SANS data show a transition from repulsive to attractive PPIs at lower applied pressure (≈200 MPa) than for the HP-SAXS data (≈275 MPa), suggesting that, with pressure holding times longer than 5 min, the applied pressure required to decrease electrostatic repulsion is lower. The 1.36 M solution presents an apparent departure from the trend of increasingly attractive PPIs with applied pressure, with an apparent uptick in b_2^* occurring above 250 MPa. The two b_2^* values at 250 and 300 MPa are however not statistically different, and prior HP-SAXS data for 1.36 M AS showed that b_2^* stabilized between 250 and 350 MPa.

The HP-SANS b_2^* data was collapsed onto a master curve and compared to the HP-SAXS results in Figure 2b. Beyond the initial reference condition (ambient pressure, AS-free), where b_2^* is similar for both, b_2^* from HP-SANS data is consistently lower than the values calculated from HP-SAXS. Attempts to shift the HP-SANS curve onto the HP-SAXS curve by simply changing the parameter G were unsuccessful, indicating a true dependence of the master curve behavior on pressure incubation time and not simply a dependence of the scaling parameter. Three effective pressure regimes are apparent in the master curves shown in Figure 2b, corresponding to 3 different slopes of the ovalbumin solution b_2^* dependency on effective pressure: 0.1–300 MPa, 300–500 MPa, and 500–700 MPa effective pressures. Figure 2a maps the data points in each regime to the corresponding applied hydrostatic pressure and assists comparisons to high-pressure data reported in the literature. In the absence of AS, and up to 300 MPa of applied pressure, the b_2^* curve is consistent with a weakening of electrostatic repulsion. The effect of the applied pressure on the phosphate buffer is expected to induce pH shifts under 0.4 units (Quinlan and Reinhart 2005). Electrostriction effects on basic protein residues also expected, because of the volume reduction associated with a more compact arrangement of water molecules around electric charges. Ovalbumin contains over 10% of basic residues, mostly present in the protein surface. The considerably negative ionization volume of Arginine and Lysine (Baldelli et al. 2024), and the proximity of the pKa of Histidine (≈6) to the solution pH, are plausible reasons for a change in the net charge of ovalbumin under pressure. Further studies are however required to confirm this hypothesis, since this effect on b_2^* can be convoluted with pressure-induced weakening of hydrophobic interactions or changes in hydration water density (Russo et al. 2017). Hydrostatic pressure-induced water screening of repulsive PPIs has also previously been suggested as a destabilizing factor in colloidal stability (Robinson and Sligar 1995; Boonyaratanakornkit et al. 2002).

In the second regime, in the presence of 0.7–1.2 M of AS, and at applied pressures up to 200 MPa, electrostatic screening by AS counterions accentuates the b_2^* dependency on effective pressure. This intermediate range of effective pressure appears to be the most sensitive to pressure holding time, where HP-SAXS and HP-SANS data differ the most. In the third regime, the increased slope of the b_2^* curve is clear for AS concentrations of 1.2 M or higher, where electrostatic screening is expected to be complete. Short-range attractive PPIs are strengthened by the AS salting out effect, and the destabilization of hydration water near hydrophobic residues by applied hydrostatic pressure (bulk water is more compressible) is expected to further enhance the b_2^* drop. Potential effects of high effective pressure on the ovalbumin form factor were not apparent from the scattering data, based on the Guinier and Kratky analyses of the HP-SANS data (Table S2 and Figure S5).

3.2 | Reversibility of Pressure-Responsive Protein Interactions From Small-Angle Neutron Scattering

The reversibility of pressure-induced effects on the protein solutions was explored by measuring ambient pressure SANS data on 10 mg/ml ovalbumin solutions before, immediately after, and 24 h after pressure treatment up to 300 MPa, taking advantage of the non-destructive nature of neutrons (see also Figure S4 and Table S3). No significant changes were reflected on the corresponding Kratky plots (Figure S6). The reduced data is shown in Figure 3, and the corresponding values of b_2^* are also compared in Figure 4 for all AS concentrations.

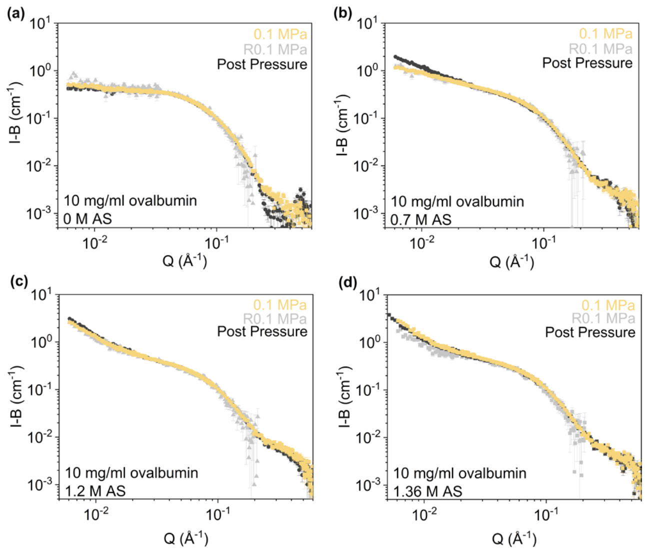

FIGURE 3 | Ambient pressure SANS profiles (background-subtracted) of 10 mg/mL ovalbumin solutions containing (a) 0 M AS, (b) 0.7 M AS, (c) 1.2 M AS, and (d) 1.36 M AS. The data shown were collected prior to pressurization (0.1 MPa, yellow squares), immediately after depressurization (R0.1 MPa, gray triangles), and aged 24 h on the bench after depressurization (post-pressure, black diamonds). Error bars are errors from scattering counting statistics and where not apparent are smaller than the symbol size.

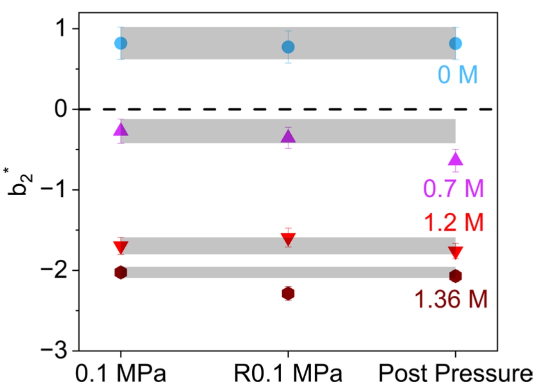

FIGURE 4 | Reduced second virial coefficients b_2^* from fits to the ambient pressure SANS profiles aged 24 h without pressurizing (0.1 MPa), 20 min after depressurization (R0.1 MPa), and 24 h after depressurization (Post Pressure) for ovalbumin solutions with varying AS concentrations as labeled. Error bars are estimated from the uncertainty in the hydrodynamic diameter (AS-free solutions) (Goldenberg and Argyle 2014) or are estimated from the fitting error in the Baxter stickiness parameter, τ_B. Gray bands are the 0.1 MPa error range for reference.

In 0 M AS solution, the agreement between the structures measured by SANS prior to and immediately after pressure treatment suggests relatively fast reversibility of the effects on PPIs. No additional aging effects were measurable 24 h later. At 0.7 M AS, the protein solution has a slightly negative b_2^* prior to pressurization, and the scattering profile appears to recover quickly upon depressurization. Upon aging at ambient pressure for 24 h, however, there is a measurable increase in the scattered intensities at low Q, indicative of protein aggregation. Exposure to high-pressure can cause protein conformational drifts, as previously documented by Weber and others (Selwood and Jaffe 2012), and trigger slow aggregation consistent with the observed HP-SANS. At 1.2 M AS, the scattering from the solution before pressurization is also consistent with the presence of protein aggregates, and pressure-triggered aggregation is not clearly distinguishable after pressurization. Finally, for the solutions at 1.36 M AS, the slope of the Q-dependence of the scattered intensities is slightly reduced immediately after pressure treatment, expected from aggregate dissociation and slow re-association (Randolph et al. 2002), but it recovers after 24 h of aging. Since this solution was treated at higher pressure than the other AS-containing solutions, a direct comparison is not possible, but the data are consistent with slower reversibility of the pressure effects. It is hypothesized that the slow reversibility is associated with the recovery from partial unfolding, since SANS can be insensitive to the effects of small conformational changes on the form factor. This is consistent with reports of increased emulsifying activity after ovalbumin treatment at 300 MPa, and that allergenicity inhibition can be partially achieved in the 250–300 MPa range (Horvitz et al. 2024).

3.3 | Extending PPI Trends to Macroscopic Rheological Behavior

3.3.1 | Dependence of Protein Solution Viscosity on Salt Concentration and on Applied Pressure

Equations (10) and (11) were used to convert ovalbumin solution viscometry data to zero-shear viscosities, as a function of AS concentration at ambient pressure. Although a different trend cannot be excluded at AS concentrations below 0.7 M, the viscosities shown in Figure 5a display an apparent monotonic increase with added salt, and are well-approximated by the expanded Jones–Dole equation (Martinus et al. 1977), commonly applied to model concentration-dependent viscosities of salt solutions:

$$\eta(C_s) = \eta_{C_s=0}\left(1 + AC_s^{0.5} + BC_s + DC_s^2\right) \tag{13}$$

where C_s is the salt concentration and $\eta_{C_s=0}$ is the salt-free viscosity. The A and B coefficients capture, respectively, effects of solute-solute interactions on viscosity, often negligible for non-electrolytes, and solute-solvent interactions. Positive B values indicate kosmotropes, such as AS, while negative values indicate chaotropes. The D coefficient accounts for ion-ion association effects in concentrated electrolyte solutions. Table 1 shows the results of the fits to Equation (13), which yield statistically similar results for the protein-free buffer and for the ovalbumin solutions. As the salt concentrations are large, compared to the concentration of ovalbumin, salt concentration effects on viscosity are expected to dominate. However, as shown in Figure 5a, the protein solution shows a consistently larger viscosity than the protein-free buffer for all AS concentrations. It was further found that the relative viscosities of ovalbumin solutions at various AS concentrations, measured by viscometry and used in Equation (4) to calculate b_2^*, are in good agreement with the reduced second osmotic virial coefficients obtained from fits to the HP-SANS data at ambient pressure (Table S7).

Version of Record at: https://doi.org/10.1111/jfpe.70088

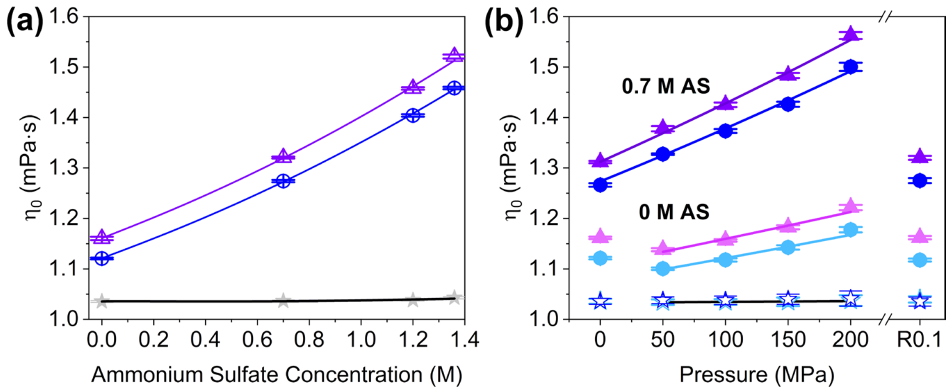

FIGURE 5 | (a) Zero-shear viscosity η_0 as a function of AS concentration, determined by capillary viscometry. Viscosities were measured for ovalbumin solutions (open triangles) and protein-free buffer (open circles). The filled stars correspond to relative viscosities. Zero-shear viscosity error bars are estimated from the variation in capillary efflux times and in density readings across 5 replicates each. The fit lines are to the expanded Jones–Dole equation. See also Table S6. (b) Zero-shear viscosity η_0 as a function of increasing applied pressure, and after returning to ambient pressure (R0.1). The viscosities were determined by HP-DWS on ovalbumin solutions containing 0 M AS and 0.7 M AS (filled triangles) and corresponding protein-free buffers (filled circles). Open stars correspond to relative viscosities for both salt concentrations (darker color for 0.7 M AS), which overlap well. The fit lines are from the Barus equation. Zero-shear viscosity error bars are 90% confidence intervals calculated from fits to the mean squared displacements (Furst and Squires 2017).

TABLE 1 | Parameter fits to the expanded Jones–Dole equation. The coefficient A was kept fixed for all fits.

Source		A $(L/mol)^{0.5}$	B (L/mol)	D $(L/mol)^2$
Capillary viscometry	Protein free buffer	0.00491	$(15.8 \pm 0.9) \times 10^{-2}$	$(4.25 \pm 0.71) \times 10^{-2}$
	Ovalbumin solutions	0.00491	$(15.9 \pm 1.1) \times 10^{-2}$	$(4.39 \pm 0.95) \times 10^{-2}$
Relative viscometry data	Ovalbumin solutions	0.00491	$(1.0 \pm 0.4) \times 10^{-2}$	$(7.4 \pm 3.1) \times 10^{-3}$

Figure 5b shows calculated viscosities from the HP-DWS data on ovalbumin solutions with 0 M AS and 0.7 M AS present (see also Figure S9). At 0 M AS, both the ovalbumin solution and protein-free buffer display a local viscosity minimum at 50 MPa, followed by an increase in viscosity with applied pressure. This is a known temperature-dependent nonmonotonic behavior. It is due to a disruption of hydrogen bond structures at relatively low pressures, observable in pure H_2O and D_2O (Horne and Johnson 2002), and expected for dilute solutions as well. At common processing temperatures for pressure-assisted thermal sterilization (50°C–90°C) (Soni and Brightwell 2022; Wimalaratne and Farid 2008), the local minimum disappears, while near 0°C temperatures used for refrigerated storage, the local minimum becomes more pronounced.

The initial viscosity measured by HP-DWS immediately after depressurization is recovered upon returning to ambient pressure. This suggests rapid reversibility of pressure effects for AS concentrations up to 0.7 M AS, as also observed by HP-SANS. Fitting the 0 M AS data beyond 50 MPa using the Barus equation yields pressure-viscosity coefficients of $(4.03 \pm 0.42) \times 10^{-4}\,\mathrm{MPa}^{-1}$ for the protein-free buffer and $(4.49 \pm 0.58) \times 10^{-4}\,\mathrm{MPa}^{-1}$ for the protein solution. Both coefficients are higher than that found for H_2O $(1 \times 10^{-4}\,\mathrm{MPa}^{-1})$. With 0.7 M AS present, the viscosity minima disappear and η_0 increases monotonically for both the ovalbumin solution and its protein-free buffer. Fitting the full 0.7 M AS pressure series to the Barus equation yields pressure-viscosity coefficients of $(7.92 \pm 0.44) \times 10^{-4}\,\mathrm{MPa}^{-1}$ for the protein-free buffer and $(8.45 \pm 0.27) \times 10^{-4}\,\mathrm{MPa}^{-1}$ for the protein solution. The larger buffer coefficients are consistent with enhanced pressure-dependence of the solution viscosity in the presence of AS, and a prevalent effect of the salt over the protein. Figure 5b also shows that the relative viscosity of ovalbumin for both AS concentrations is nearly identical.

3.3.2 | Dependence of Protein Relative Viscosity on Effective Pressure

Plotting the Baxter stickiness parameter (Figure 2b, inset) as a function of the effective pressure reveals that the strength of interaction follows a Barus-like behavior with a large pressure-viscosity coefficient $\alpha_\tau \sim 4 \times 10^{-3}\,\mathrm{MPa}^{-1}$. Following Equation (12), relative viscosities η_r were calculated from fitted Baxter stickiness parameters for each HP-SANS data set. Predicted values are shown in Figure 6, along with the best fit line to a normalized Barus equation as:

$$\eta_r\left(P_{eff}\right) = \eta_{r,0} e^{\alpha_r P_{eff}} \tag{14}$$

where α_r is a relative pressure-viscosity coefficient and $\eta_{r,0}$ is the protein relative viscosity at ambient pressure. It was assumed that any correlations between the protein and solvent viscosities are negligible. Hydrostatic pressure has additionally been replaced by the effective pressure, P_{eff}. Fitting Equation (14) to predicted η_r data yields a relative pressure-viscosity coefficient of $(8.47 \pm 0.36) \times 10^{-6}\,\mathrm{MPa}^{-1}$. Figure 6 also shows how the fit line

Version of Record at: https://doi.org/10.1111/jfpe.70088

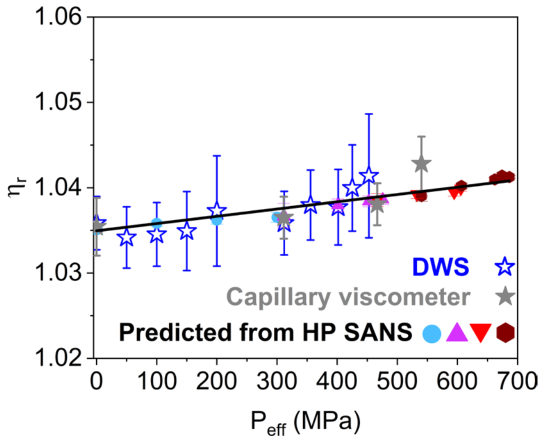

FIGURE 6 | Relative viscosity η_r for the measured experimental conditions as a function of effective pressure. Filled symbols, matching those in Figure 2, are predicted η_r from HP-SANS fitted Baxter stickiness parameters, τ_B. Stars are calculated η_r from experimental measurements at ambient pressure using a capillary viscometer and density meter (gray filled symbols) and at elevated pressure using HP-DWS (blue open symbols). Error bars are calculated from uncertainty in experimental measurements. The fit line is to the normalized Barus equation. Schematic representation of the relevance of holding time in measurements involving pressure effects on protein structure. Pressure is represented generically by a press. Protein molecules are depicted in green, and the shortening of the range of interaction is shown through shorter distances between protein molecules.

to the normalized Barus equation compares to relative viscosity data viscometry and HP-DWS measurements. The experimentally determined trend for HP-SANS matches well with the predicted trend from HP-DWS data, with a pressure viscosity coefficient of $(9.93 \pm 2.09) \times 10^{-6}\,\mathrm{MPa}^{-1}$. Despite the larger variability in the rheological data, the two fitted coefficients statistically agree.

The agreement between relative viscosities and b_2^* calculated from different techniques has important implications for the validation of the comparison between HP-SAXS and HP-SANS data to investigate the effects of 5 min and 20 min pressure incubation times, respectively. The scattering data series for each AS concentration are collected in a sequence of pressure steps after the incubation time, but data collection times are significantly shorter for SAXS (less than 1 min) than for SANS (up to 1 h). Potential effects of hysteresis on the two measurements, where SANS data at the highest-pressure steps was collected for samples exposed to pressure for significantly longer time during data collection, were considered. The agreement between viscometry, HP-DWS and HP-SANS data (where data collection times differ significantly) confirms however that, after the initial pressure incubation prior to the start of the data collection, HP-SANS data were measured on equilibrated solutions. This excludes hysteresis effects on PPIs beyond 20 min of applied pressure incubation. As shown in Figure 2b, data collected on ovalbumin solutions with 0.7 M AS are found in the P_{eff} range where larger differences were observed for b_2^* from HP-SAXS and HP-SANS data.

The relative viscosity trend shown in Figure 6, cross-validated between multiple complementary characterization approaches, shows a statistically real increase in resistance to flow as salt concentration or pressure is increased. The SANS scattering profiles detected aggregation and where such larger particle formation is known to hinder fluidity (Heinen et al. 2012). Increasing relative viscosity has consistently been correlated with a transition from weak interparticle association to the beginning of protein oligomerization to the onset of crowding or bulk aggregation (Moron et al. 2022; Parmar and Muschol 2009; Roosen-Runge et al. 2020).

4 | Conclusions

This study builds on a previous investigation of combined effects of applied pressure and dissolved salt on protein solution from molecular scale to macroscopic behavior. Longer pressure holding times enhance the applied pressure effect on ovalbumin PPIs, which grow more attractive. HP-DWS or time-resolved SANS measurements can produce further information on the effects of relatively long pressure incubation times, relevant to food and formulation processing. Pressure effects in the presence of salt are not entirely reversible upon depressurization. Most experimental data are collected up to 10 min after pressure treatment and can fail to capture pressure-triggered slow processes that develop over hours or days, including the irreversible formation of soluble protein clusters or aggregates. This has major implications for viscosity and allergenicity, among other properties.

Microrheological and viscometry measurements are shown to match well with the predicted viscosity trends from HP-SANS, with an increase in protein relative viscosity as effective pressure increases. HP-DWS is an effective and fast screening tool for measuring formulation behavior at lower salt concentrations where tracer particles remain stable. HP-SANS allows for accurate measurement of protein behavior and good prediction of formulation viscosity at higher salt concentrations. Solution viscosity is a key process parameter, and an expansion of the current approach to more complex formulations or higher protein concentrations is expected, as improved methods are developed to fit structure factors and contrast variation techniques are used to deconvolute neutron scattering data. Salt and protein concentration regimes where DWS and SANS can be compared provide cross-validation, while stability screening in the conditions where each technique is optimal will contribute to more efficient product development and provide critical data for developing predictive models.

The empirical correlation of PPIs with the effective pressure is shown to hold broadly for multiple incubation times. Further analysis shows that the interprotein interaction potential follows a Barus-like scaling with a large pressure-viscosity coefficient compared with water and typical organic lubricants. This observation is powerfully reflected in the effects of salt and pressure on relative solution viscosity, even at dilute protein concentration, which is shown to also follow the Barus equation. The relative viscosity trends suggest that a combination of applied pressure and dissolved salt can be used to adjust the extent of protein association and dictate phase behavior, providing opportunities for product and process development optimization.

Author Contributions

S.C.M.T., N.J.W., E.M.F., and A.M.L. initiated the research project. S.C.M.T., N.J.W., E.M.F., A.M.L., and E.P.G. reviewed the manuscript. B.P., E.P.G., and S.C.M.T. collected and reduced the scattering data, and B.P. and S.C.M.T. analyzed the scattering data. B.P. collected and analyzed the viscometry and microrheology data, fitted the scattering data, and calculated the master curves. All authors contributed to the writing of the manuscript. B.P. generated the table of contents graphic.

Acknowledgments

This work was prepared under cooperative agreement #70NANB20H133 from NIST, U.S. Department of Commerce. We acknowledge the support of the National Institute of Standards and Technology, U.S. Department of Commerce, in providing the research facilities used in this work. We acknowledge the support of the Australian Centre for Neutron Scattering, ANSTO and the Australian Government through the National Collaborative Research Infrastructure Strategy, in supporting the neutron research infrastructure used in this work via ACNS proposal P16562. We thank Cedric Gagnon (University of Maryland/NIST), John Barker (NIST), and Amy Shumack (Australian Center for Neutron Scattering) for assistance with preparing the high-pressure SANS sample environment for QUOKKA. This work benefitted from the use of the SasView software, which was originally developed by the DANSE project under NSF Award DMR-050547.

Certain instruments and software are identified to foster understanding. Such identification does not imply recommendation or endorsement by the National Institute of Standards and Technology, nor does it imply that the instruments and software identified are necessarily the best available for the purpose. The statements, findings, conclusions, and recommendations are those of the authors and do not necessarily reflect the view of NIST, the Australian Centre for Neutron Scattering, or the U.S. Department of Commerce.

Conflicts of Interest

The authors declare no conflicts of interest.

Data Availability Statement

The neutron scattering data collected at the National Institute of Standards and Technology, that supports the findings of this study, is openly available at the NIST Center for Neutron Research Data Repository at https://dx.doi.org/10.18434/T4201B?urlappend=ng7sans/202009, reference number NG7SANS42. The neutron scattering data collected at the Australian Center for Neutron Scattering, and the Diffusing Wave Spectroscopy data collected at the University of Delaware, are available from the authors upon reasonable request.

References

Abbas, K. A., S. M. Abdulkarim, A. M. Saleh, and M. Ebrahimian. 2010. "Suitability of Viscosity Measurement Methods for Liquid Food Variety and Applicability in Food Industry—A Review." *Journal of Food, Agriculture and Environment* 8, no. 3–4: 100–107.

Abeyrathne, E. D., H. Y. Lee, and D. U. Ahn. 2013. "Egg White Proteins and Their Potential Use in Food Processing or as Nutraceutical and Pharmaceutical Agents—A Review." *Poultry Science* 92, no. 12: 3292–3299. https://doi.org/10.3382/ps.2013-03391.

Allai, F. M., Z. R. A. A. Azad, N. A. Mir, and K. Gul. 2023. "Recent Advances in Non-Thermal Processing Technologies for Enhancing Shelf Life and Improving Food Safety." *Applied Food Research* 3, no. 1: 100258. https://doi.org/10.1016/j.afres.2022.100258.

Amsasekar, A., R. S. Mor, A. Kishore, A. Singh, and S. Sid. 2022. "Impact of High Pressure Processing on Microbiological, Nutritional and Sensory Properties of Food: A Review." *Nutrition & Food Science* 52, no. 6: 996–1017. https://doi.org/10.1108/Nfs-08-2021-0249.

Baldelli, A., J. Shi, A. Singh, et al. 2024. "Effect of High-Pressure on Protein Structure, Refolding, and Crystallization." *Food Chemistry Advances* 5: 100741. https://doi.org/10.1016/j.focha.2024.100741.

Barus, C. 1893. "Isothermals, Isopiestics and Isometrics Relative to Viscosity." *American Journal of Science* 45, no. 266: 87–96.

Boonyaratanakornkit, B. B., C. B. Park, and D. S. Clark. 2002. "Pressure Effects on Intra- and Inter-Molecular Interactions Within Proteins." *Biochimica et Biophysica Acta-Protein Structure and Molecular Enzymology* 1595, no. 1–2: 235–249. https://doi.org/10.1016/S0167-4838(01)00347-8.

Charlier, C., T. R. Alderson, J. M. Courtney, J. Ying, P. Anfinrud, and A. Bax. 2018. "Study of Protein Folding Under Native Conditions by Rapidly Switching the Hydrostatic Pressure Inside an NMR Sample Cell." *Proceedings of the National Academy of Sciences of the United States of America* 115, no. 18: E4169–E4178. https://doi.org/10.1073/pnas.1803642115.

Chen, Q., L. Dong, Y. Li, et al. 2024. "Research Advance of Non-Thermal Processing Technologies on Ovalbumin Properties: The Gelation, Foaming, Emulsification, Allergenicity, Immunoregulation and Its Delivery System Application." *Critical Reviews in Food Science and Nutrition* 64, no. 20: 7045–7066. https://doi.org/10.1080/10408398.2023.2179969.

Couch, M. A., and D. M. Binding. 2000. "High Pressure Capillary Rheometry of Polymeric Fluids." *Polymer* 41, no. 16: 6323–6334. https://doi.org/10.1016/S0032-3861(99)00865-4.

Dennis, K. A., Y. Gao, A. Phatak, P. F. Sullivan, and E. M. Furst. 2020. "Design, Operation, and Validation of a Microrheology Instrument for High-Pressure Linear Viscoelasticity Measurements." *Journal of Rheology* 64, no. 1: 205–212. https://doi.org/10.1122/1.5126682.

Diwan, D., M. Sharma, M. Tabatabaei, and V. K. Gupta. 2021. "Ovalbumin Production Without Poultry." *Nature Food* 2: 924–925. https://doi.org/10.1038/s43016-021-00438-y.

Dong, L., X. Lu, X. A. Zeng, and S. Lin. 2024. "Regulation of Ovalbumin Allergenicity and Structure-Activity Relationship Analysis Based on Pulsed Electric Field Technology." *International Journal of Biological Macromolecules* 261, no. 1: 129695. https://doi.org/10.1016/j.ijbiomac.2024.129695.

Doucet, M., J. H. Cho, G. Alina, et al. 2022. *SasView Version 5.0.5* Zenodo. https://doi.org/10.5281/zenodo.6331344.

Dumetz, A. C., A. M. Chockla, E. W. Kaler, and A. M. Lenhoff. 2008. "Protein Phase Behavior in Aqueous Solutions: Crystallization, Liquid-Liquid Phase Separation, Gels, and Aggregates." *Biophysical Journal* 94, no. 2: 570–583. https://doi.org/10.1529/biophysj.107.116152.

Finnigan, J. A., and D. J. Jacobs. 1971. "Light Scattering by Ellipsoidal Particles in Solution." *Journal of Physics D: Applied Physics* 4, no. 1: 72–77. https://doi.org/10.1088/0022-3727/4/1/310.

Förster, P., F. Werner, and A. Delgado. 2002. "On the Pressure Dependence of the Viscosity of Aqueous Sugar Solutions." *Rheologica Acta* 41, no. 4: 369–374. https://doi.org/10.1007/s00397-002-0238-y.

Furst, E. M., and T. M. Squires. 2017. *Microrheology*. Oxford University Press. https://doi.org/10.1093/oso/9780199655205.001.0001.

Garting, T., and A. Stradner. 2018. "Optical Microrheology of Protein Solutions Using Tailored Nanoparticles." *Small* 14, no. 46: 1801548. https://doi.org/10.1002/smll.201801548.

Glinka, C. J., J. G. Barker, B. Hammouda, S. Krueger, J. J. Moyer, and W. J. Orts. 1998. "The 30 m Small-Angle Neutron Scattering Instruments at the National Institute of Standards and Technology." *Journal of Applied Crystallography* 31, no. 3: 430–445. https://doi.org/10.1107/S0021889897017020.

Goldenberg, D. P., and B. Argyle. 2014. "Self Crowding of Globular Proteins Studied by Small-Angle X-Ray Scattering." *Biophysical Journal* 106, no. 4: 895–904. https://doi.org/10.1016/j.bpj.2013.12.004.

Greene, D. G., S. Modla, N. J. Wagner, S. I. Sandler, and A. M. Lenhoff. 2015. "Local Crystalline Structure in an Amorphous Protein Dense Phase." *Biophysical Journal* 109, no. 8: 1716–1723. https://doi.org/10.1016/j.bpj.2015.08.023.

Hayashi, S., K. Masuhara, S. Mia, S. Morita, and N. Ohno. 2008. "Prediction of Pressure-Viscosity Coefficient of Mixtures." *Tribology Online* 3, no. 2: 86–89. https://doi.org/10.2474/trol.3.86.

Heinen, M., F. Zanini, F. Roosen-Runge, et al. 2012. "Viscosity and Diffusion: Crowding and Salt Effects in Protein Solutions." *Soft Matter* 8, no. 5: 1404–1419. https://doi.org/10.1039/c1sm06242e.

Hopkins, J. B., and R. E. Thorne. 2016. "Quantifying Radiation Damage in Biomolecular Small-Angle X-Ray Scattering." *Journal of Applied Crystallography* 49, no. Pt 3: 880–890. https://doi.org/10.1107/S1600576716005136.

Horne, R. A., and D. S. Johnson. 2002. "The Viscosity of Water Under Pressure." *Journal of Physical Chemistry* 70, no. 7: 2182–2190. https://doi.org/10.1021/j100879a018.

Horvitz, S., C. Arroqui, and P. Vírseda. 2024. "Mild High Hydrostatic Pressure Processing: Effects on Techno-Functional Properties and Allergenicity of Ovalbumin." *Journal of Food Engineering* 364: 111797. https://doi.org/10.1016/j.jfoodeng.2023.111797.

Ianeselli, L., F. Zhang, M. W. Skoda, et al. 2010. "Protein-Protein Interactions in Ovalbumin Solutions Studied by Small-Angle Scattering: Effect of Ionic Strength and the Chemical Nature of Cations." *Journal of Physical Chemistry B* 114, no. 11: 3776–3783. https://doi.org/10.1021/jp9112156.

Josephson, L. L., E. M. Furst, and W. J. Galush. 2016. "Particle Tracking Microrheology of Protein Solutions." *Journal of Rheology* 60, no. 4: 531–540. https://doi.org/10.1122/1.4948427.

Kim, A. J., V. N. Manoharan, and J. C. Crocker. 2005. "Swelling-Based Method for Preparing Stable, Functionalized Polymer Colloids." *Journal of the American Chemical Society* 127, no. 6: 1592–1593. https://doi.org/10.1021/ja0450051.

Kline, S. R. 2006. "Reduction and Analysis of SANS and USANS Data Using IGOR pro." *Journal of Applied Crystallography* 39, no. 6: 895–900. https://doi.org/10.1107/S0021889806035059.

Knorr, D. 2002. "High Pressure Processing for Preservation, Modification and Transformation of Foods." *High Pressure Research* 22, no. 3–4: 595–599. https://doi.org/10.1080/08957950212411.

Kotlarchyk, M., and S. H. Chen. 1983. "Analysis of Small-Angle Neutron-Scattering Spectra From Polydisperse Interacting Colloids." *Journal of Chemical Physics* 79, no. 5: 2461–2469. https://doi.org/10.1063/1.446055.

Lundblad, R. L., and F. Macdonald, eds. 2018. *Handbook of Biochemistry and Molecular Biology*. Vol. 188. CRC Press. https://doi.org/10.1201/b21846.

Marjanović, D., S. Jovanović, A. Baars, and M. Barać. 2011. "Effects of High Hidrostatic Pressure on the Viscosity of β-Lactoglobulin Solution." *Mljekarstvo* 61, no. 2: 135–144.

Martinus, N., C. D. Sinclair, and C. A. Vincent. 1977. "The Extended Jones-Dole Equation." *Electrochimica Acta* 22: 1183–1187.

McGlynn, J. A., N. Wu, and K. M. Schultz. 2020. "Multiple Particle Tracking Microrheological Characterization: Fundamentals, Emerging Techniques and Applications." *Journal of Applied Physics* 127, no. 20: 201101. https://doi.org/10.1063/5.0006122.

Monkos, K. 2000. "Viscosity Analysis of the Temperature Dependence of the Solution Conformation of Ovalbumin." *Biophysical Chemistry* 85, no. 1: 7–16. https://doi.org/10.1016/s0301-4622(00)00127-7.

Moron, M., A. Al-Masoodi, C. Lovato, et al. 2022. "Gelation Dynamics Upon Pressure-Induced Liquid-Liquid Phase Separation in a Water-Lysozyme Solution." *Journal of Physical Chemistry B* 126, no. 22: 4160–4167. https://doi.org/10.1021/acs.jpcb.2c01947.

Ngamlerst, C., P. Prangthip, B. Leelawat, S. Supawong, and S. Vatthanakul. 2022. "A Vital Role of High-Pressure Processing in the Gel Forming on New Healthy Egg Pudding Through Texture, Microstructure, and Molecular Impacts." *Food* 11, no. 17: 2555. https://doi.org/10.3390/foods11172555.

Parmar, A. S., and M. Muschol. 2009. "Hydration and Hydrodynamic Interactions of Lysozyme: Effects of Chaotropic Versus Kosmotropic Ions." *Biophysical Journal* 97, no. 2: 590–598. https://doi.org/10.1016/j.bpj.2009.04.045.

Paul, B., E. M. Furst, A. M. Lenhoff, N. J. Wagner, and S. C. M. Teixeira. 2023. "Combined Effects of Pressure and Ionic Strength on Protein-Protein Interactions: An Empirical Approach." *Biomacromolecules* 25, no. 1: 338–348. https://doi.org/10.1021/acs.biomac.3c01001.

Quinlan, R. J., and G. D. Reinhart. 2005. "Baroresistant Buffer Mixtures for Biochemical Analyses." *Analytical Biochemistry* 341, no. 1: 69–76. https://doi.org/10.1016/j.ab.2005.03.002.

Randolph, T. W., M. Sefeldt, and J. F. Carpenter. 2002. "High Hydrostatic Pressure as a Tool to Study Protein Aggregation and Amyloidosis." *Biochimica et Biophysica Acta (BBA) - Protein Structure and Molecular Enzymology* 1595, no. 1–2: 224–234. https://doi.org/10.1016/S0167-4838(01)00346-6.

Rastogi, N. K. 2013. *Recent Developments in High Pressure Processing of Foods*. Springer.

Robinson, C. R., and S. G. Sligar. 1995. "Hydrostatic and Osmotic Pressure as Tools to Study Macromolecular Recognition." *Methods in Enzymology* 259: 395–426. https://doi.org/10.1016/0076-6879(95)59054-4.

Roosen-Runge, F., A. Gulotta, S. Bucciarelli, et al. 2020. "Crowding in the Eye Lens: Modeling the Multisubunit Protein Beta-Crystallin With a Colloidal Approach." *Biophysical Journal* 119, no. 12: 2483–2496. https://doi.org/10.1016/j.bpj.2020.10.035.

Rostamabadi, H., V. Chaudhary, N. Chhikara, et al. 2023. "Ovalbumin, an Outstanding Food Hydrocolloid: Applications Technofunctional Attributes, and Nutritional Facts, A Systematic Review." *Food Hydrocolloids* 139: 108514. https://doi.org/10.1016/j.foodhyd.2023.108514.

Russo, D., A. Laloni, A. Filabozzi, and M. Heyden. 2017. "Pressure Effects on Collective Density Fluctuations in Water and Protein Solutions." *Proceedings. National Academy of Sciences. United States of America* 114, no. 43: 11410–11415. https://doi.org/10.1073/pnas.1705279114.

Selwood, T., and E. K. Jaffe. 2012. "Dynamic Dissociating Homo-Oligomers and the Control of Protein Function." *Archives of Biochemistry and Biophysics* 519, no. 2: 131–143. https://doi.org/10.1016/j.abb.2011.11.020.

Soni, A., and G. Brightwell. 2022. "Effect of Hurdle Approaches Using Conventional and Moderate Thermal Processing Technologies for Microbial Inactivation in Fruit and Vegetable Products." *Food* 11, no. 12: 1811. https://doi.org/10.3390/foods11121811.

Teixeira, S. C. M. 2019. "High-Pressure Small-Angle Neutron Scattering for Food Studies." *Current Opinion in Colloid & Interface Science* 42: 99–109. https://doi.org/10.1016/j.cocis.2019.05.001.

Teixeira, S. C. M., J. B. Leao, C. Gagnon, and M. A. McHugh. 2018. "High Pressure Cell for Bio-SANS Studies Under Sub-Zero Temperatures or Heat Denaturing Conditions." *Journal of Neutron Research* 20, no. 1–2: 11–21. https://doi.org/10.3233/Jnr-180057.

Ullner, M., K. Qamhieh, and B. Cabane. 2018. "Osmotic Pressure in Polyelectrolyte Solutions: Cell-Model and Bulk Simulations." *Soft Matter* 14, no. 28: 5832–5846. https://doi.org/10.1039/c8sm00654g.

Wagner, N. J., and J. Mewis. 2012. *Colloidal Suspension Rheology*. Cambridge University Press.

Weitz, D., and D. Pine. 1993. *Dynamic Light Scattering: The Method and Some Applications*. Oxford University Press.

Wimalaratne, S. K., and M. M. Farid. 2008. "Pressure Assisted Thermal Sterilization." *Food and Bioproducts Processing* 86, no. C4: 312–316. https://doi.org/10.1016/j.fbp.2007.08.001.

Winter, R. 2015. *Pressure Effects on the Intermolecular Interaction Potential of Condensed Protein Solutions*, 151–176. Springer Netherlands. https://doi.org/10.1007/978-94-017-9918-8_8.

Wood, K., J. P. Mata, C. J. Garvey, et al. 2018. "QUOKKA, the Pinhole Small-Angle Neutron Scattering Instrument at the OPAL Research Reactor, Australia: Design, Performance, Operation and Scientific Highlights." *Journal of Applied Crystallography* 51, no. 2: 294–314. https://doi.org/10.1107/S1600576718002534.

Xu, X., D. Gagne, J. M. Aramini, and K. H. Gardner. 2021. "Volume and Compressibility Differences Between Protein Conformations Revealed by High-Pressure NMR." *Biophysical Journal* 120, no. 5: 924–935. https://doi.org/10.1016/j.bpj.2020.12.034.

Supporting Information

Additional supporting information can be found online in the Supporting Information section.